ADVANCES IN ATMOSPHERIC SCIENCES, VOL. 31, JULY 2014, 863–878

The Southern Annular Mode (SAM) in PMIP2 Simulations of the Last Glacial Maximum

Seong-Joong KIM[1], LÜ Junmei*[2], and Baek-Min KIM[1]

[1]*Korea Polar Research Institute, KORDI, PO Box* 32, *Incheon* 406-840, *Korea*
[2]*Chinese Academy of Meteorological Sciences, Beijing* 100081

(Received 17 September 2013; revised 04 December 2013; accepted 23 December 2013)

ABSTRACT

The increasing trend of the Southern Annular Mode (SAM) in recent decades has influenced climate change in the Southern Hemisphere (SH). How the SAM will respond increased greenhouse gas concentrations in the future remains uncertain. Understanding the variability of the SAM in the past under a colder climate such as during the Last Glacial Maximum (LGM) might provide some understanding of the response of the SAM under a future warmer climate. We analyzed the changes in the SAM during the LGM in comparison to pre-industrial (PI) simulations using five coupled ocean–atmosphere models (CCSM, FGOALS, IPSL, MIROC, HadCM) from the second phase of the Paleoclimate Modelling Intercomparison Project (PMIP2). In CCSM, MIROC, IPSL, and FGOALS, the variability of the simulated SAM appears to be reduced in the LGM compared to the PI simulations, with a decrease in the standard deviation of the SAM index. Overall, four out of the five models suggest a weaker SAM amplitude in the LGM consistent with a weaker SH polar vortex and westerly winds found in some proxy records and model analyses. The weakening of the SAM in the LGM was associated with an increase in the vertical propagation of Rossby waves in southern high latitudes.

Key words: Southern Annular Mode, Last Glacial Maximum, PMIP2, Southern Hemisphere westerly winds

Citation: Kim, S.-J., J. M. Lü, and B.-M. Kim, 2014: The Southern Annular Mode (SAM) in PMIP2 simulations of the Last Glacial Maximum. *Adv. Atmos. Sci.*, **31**(4), 863–878, doi: 10.1007/s00376-013-3179-8.

1. Introduction

Over the past several decades, a substantial temperature increase has been observed in West Antarctica, especially the Antarctic Peninsula, whereas very little change or even a slight cooling is found over East Antarctica (Turner et al., 2005; Chapman and Walsh, 2007; Monaghan et al., 2008; Steig et al., 2009; O'Donnell et al., 2011; Schneider et al., 2012). The pattern of Antarctic temperature change with marked warming in the Antarctic Peninsula and slight cooling in East Antarctica has been attributed to the increased strength of the Southern Hemisphere (SH) polar vortex associated with the positive trends of the Southern Annular Mode (SAM) (Kwok and Comiso, 2002; Thompson and Solomon, 2002; Gillett and Thompson, 2003; Marshall, 2003; Marshall et al., 2004; Marshall and Connolley, 2006).

As the leading mode of low-frequency atmospheric variability in the SH, the SAM exhibits an equivalent barotropic vertical structure extending from the lower stratosphere to the surface and a zonally symmetric structure and leads to the exchange of atmospheric mass between the mid and high latitudes (Gong and Wang, 1999; Thompson and Wallace, 2000). The positive SAM polarity is associated with the stronger westerly winds at low levels, which enhances the northward Ekman divergence over the Southern Ocean (SO) and yields a more extensive sea ice cover (Hall and Visbeck, 2002) and a stronger oceanic upwelling (Lefebvre et al., 2004). The positive SAM polarity also leads to a decrease in rainfall over southwestern Australia (Karoly, 2003) and over southeast South America (Silvestri and Vera, 2003), and the increase in the transport of the Antarctic Circumpolar Current through Drake Passage (Meredith et al., 2004).

Over the past 40 years, the SAM polarity has been increasing toward a high-index state, until around the year 2000 (Hurrell and van Loon, 1994; Jones and Widmann, 2003; Marshall, 2003). The recent increase in the SAM polarity is mainly due to the decrease in stratospheric ozone (Thompson and Solomon, 2002; Gillett and Thompson, 2003; Gillett et al., 2006; Keeley et al., 2007; Son et al., 2008) and in part by the increase in greenhouse gas concentration (Kushner et al., 2001; Shindell and Schmidt, 2004; Cai and Cowan, 2007). In the future, it is projected that the SAM will not change essentially, but rather be superimposed on the forced climate change (Fyfe et al., 1999; Karpechko et al., 2010; Son et al., 2010; Polvani et al., 2011). The future projection of the SAM's status is a prime concern because its state is directly related to the atmospheric and oceanic dynamics in the South-

* Corresponding author: LÜ Junmei
Email: wind-ljm@163.com

ern Ocean. However, there are only a few studies available on this topic and the status of the SAM under a future warmer climate remains highly uncertain. As an alternative, the analysis of past climates can provide useful information regarding the future change of the SAM under increased CO_2.

To assess the ability of models to reproduce the climate that is different from present day and to investigate how the climate behaved in the past, the Paleoclimate Modelling Intercomparison Project (PMIP1) was launched in the mid1990s (Joussaume and Taylor, 2000). In the first phase of the PMIP, atmospheric general circulation models (AGCMs) with specified SST and calculated SST using slab ocean models were used to simulate the climate for the mid-Holocene at 6000 years before present (6 kyr BP) and the last glacial maximum (LGM) at 21000 years before present (21 kyr BP). In the second phase of the PMIP started in 2002 the feedbacks of ocean dynamics and land surface vegetation were included by coupling AGCMs with 3-D oceanic GCMs (Harrison et al., 2002; Crucifix et al., 2005). The PMIP2 achieved considerable success in increasing our understanding of climate change on the LGM such as the comparison of proxy records with model results over the North Atlantic and Eurasia (Kageyama et al., 2006; Ramstein et al., 2007), over China (Jiang et al., 2011), and the surface ocean (Otto-Bliesner et al., 2009), large-scale features and tropical feedbacks (Braconnot et al., 2007a, 2007b), precipitation and heat balance (Yanase and Abe-Ouchi, 2007; Murakami et al., 2008), Northern Hemisphere (NH) storm tracks and climate variability (Laîné et al., 2008; Li and Battisti, 2008; Pausata et al., 2009), East Asian monsoon (Jiang and Lang, 2010), ocean thermohaline circulation (Otto-Bliesner et al., 2007; Weber et al., 2007), SH westerlies (Rojas et al., 2008), and Arctic Oscillation (Lü et al., 2010).

Despite the considerable success in understanding LGM climate through the PMIP2's efforts, the climate variability in the SH remains uncertain. In particular, the intensity of the SAM and the link between its variability and the mean state of the SH climate are highly controversial and not yet completely understood. As mentioned above, the intensity of the SAM is directly related to the strength of SH westerly winds, which is believed to have played an important role in reducing the atmospheric CO_2 concentration during the LGM by its northward shift and weakening of the Ekman divergence in the SO (Sigman and Boyle, 2000; Toggweiler et al., 2006; Anderson et al., 2009; Toggweiler, 2009; Sigman et al., 2010). Although the intensity of the SAM and the link between its variability and the mean state of SH climate are critical for Antarctic climate change and atmospheric and oceanic circulations, the mechanism underpinning the modulation of SAM variability has not yet been fully studied. Here we investigate the variability of the SAM and its role in atmospheric circulations under the cold LGM climate using simulation results from PMIP2 to gain a better understanding of the physical mechanisms driving the SAM.

2. Models and experiments

In this study, we used results from five atmosphere–ocean coupled models: NCAR Community Climate System Model version 3 (CCSM); LASG/IAP Flexible Global Ocean–Atmosphere–Land System Model (FGOALS); L'Institut Pierre-Simon Laplace-CM4 (IPSL); Model for Interdisciplinary Research on Climate version 3.2 (MIROC); and the third climate configuration of the Met Office Unified Model with Met Office Surface Exchanges Scheme version 2 (HadCM3M2). Details of these models and associated references are summarized in Table 1. CCSM, MIROC, and FGOALS use the same atmospheric resolution of T42 (2.5° in Gaussian grid), while oceanic resolutions vary from 0.3° to 1° zonally and 1° to 1.4° meridionally. The simulation years that were used in the analyses are from year 11 to year 35 for CCSM and from year 41 to year 90 for the other three models' results.

Austral winter (June–July–August, JJA) seasonal mean and variability of SAM obtained by the LGM simulations are compared with those from the preindustrial (PI) simulations because the westerly polar vortex is strongest during those times. PMIP2 applied standard forcings and boundary conditions for the PI and LGM simulations for a fair comparison between models (Table 2). The PI simulations used forcings at 1750 AD and LGM simulations used forcings reconstructed for ∼21 000 years ago (21 kyr BP). For the ice sheet topography during the LGM, ICE-5G (5th generation of ice-sheet reconstruction) data were used and sea level was lowered to account for the ice sheet volume. The present river routings were used in all LGM simulations except for the HadCM. Orbital parameters were calculated following Berger (1978). Atmospheric greenhouse gases were

Table 1. PMIP2 models used in the SAM analysis

Model version	Institute	Atmosphere resolution	Ocean resolution	Reference
CCSM3	National Center for Atmospheric Research	T42 2.8° (lat) ×2.8° (lon)	0.3°–1° (lat) ×1° (lon)	Otto-Bliesner et al. (2006a, b)
HadCM3M2	UK Met Office Hadley Center, UK	2.5° (lat) ×3.75° (lon)	1.25° (lat) ×1.25° (lon)	Gordon et al. (2000)
MIROC3.2	Center for Climate System Research (University of Tokyo), Frontier Research Center for Global Change, Japan	T42 2.8° (lat) ×2.8° (lon)	0.5°–1.4° (lat) ×1.4° (lon)	K-1 Model Developers (2004)
IPSL-CM4	Institute Pierre Simon Laplace, France	2.5° (lat) ×3.75° (lon)	1°–2° (lat) ×2° (lon)	Marti et al. (2005)
FGOALS	LASG/Institute of Atmospheric Physics, China	T42 2.8° (lat) ×2.8° (lon)	1° (lat) ×1° (lon)	Yu et al. (2004)

Table 2. PMIP2 forcing and boundary conditions for the LGM and preindustrial simulations.

	Preindustrial	LGM
CO_2 (ppm)	280	185
CH_4 (ppv)	760	350
N_2O (ppv)	270	200
Eccentricity	0.16724	0.018994
Obliquity	23.446	22.949
Precession	102.04	114.42
Ice sheet	Present	Ice-5G
Land Mask	Present	Ice-5G
Vegetation	Present	Present

low in concentration during the LGM according to Greenland and Antarctic ice core reconstructions (Flückiger et al., 1999; Dällenbach et al., 2000; Monnin et al., 2001) Detailed values of boundary conditions used in the PI and LGM simulations are listed in Table 2 (see also the PMIP2 website: http://pmip2.lsce.ipsl.fr).

3. Results

3.1. *Present and LGM climate*

In this paper we focus on the climate change over Antarctica and its associated change in the SAM during austral winter. Figure 1 displays the winter mean JJA sea level pressure (SLP) from NCEP/NCAR reanalysis (Fig. 1f) and the PI simulations (Figs. 1a–e). We used the NCEP/NCAR reanalysis data for the period 1951–2002. In the reanalysis data, the anticyclonic highs are developed over midlatitudes and around the Antarctic continent. The lowpressure systems referred to as the Antarctic trough form a continuous zonal belt with very low values of surface pressure. Toward the South Pole, the SLP tends to increase, but due to the high altitude of more than 4000 m in places at the rim of Antarctica the reanalyzed SLP should not be regarded as meaningful.

In the PI simulation, the anticyclones are generally well reproduced in their intensity and position in all five coupled models. In terms of the low pressures in the Antarctic trough, their intensities are stronger than the reanalysis in CCSM, HadCM, and MIROC, while they are weaker in IPSL and FGOALS. Toward the interior of the Antarctic continent, SLP increases gradually, but it is not as high as in the reanalysis data, except for IPSL which reproduces the PI SLP as quite close to the reanalysis. As mentioned the SLP in the interior of the Antarctic continent is not meaningful. Overall, all the models capture the low pressures over the rim of Antarctica and high pressures in the interior. Though the magnitude of the low and high pressure systems are different between models and reanalysis data, all the coupled models capture the features of the present SLP found in the reanalysis data.

The simulated winter climatology of vertical cross sections of the zonal-mean zonal winds, temperature, and geopotential height are compared with those of the observed in

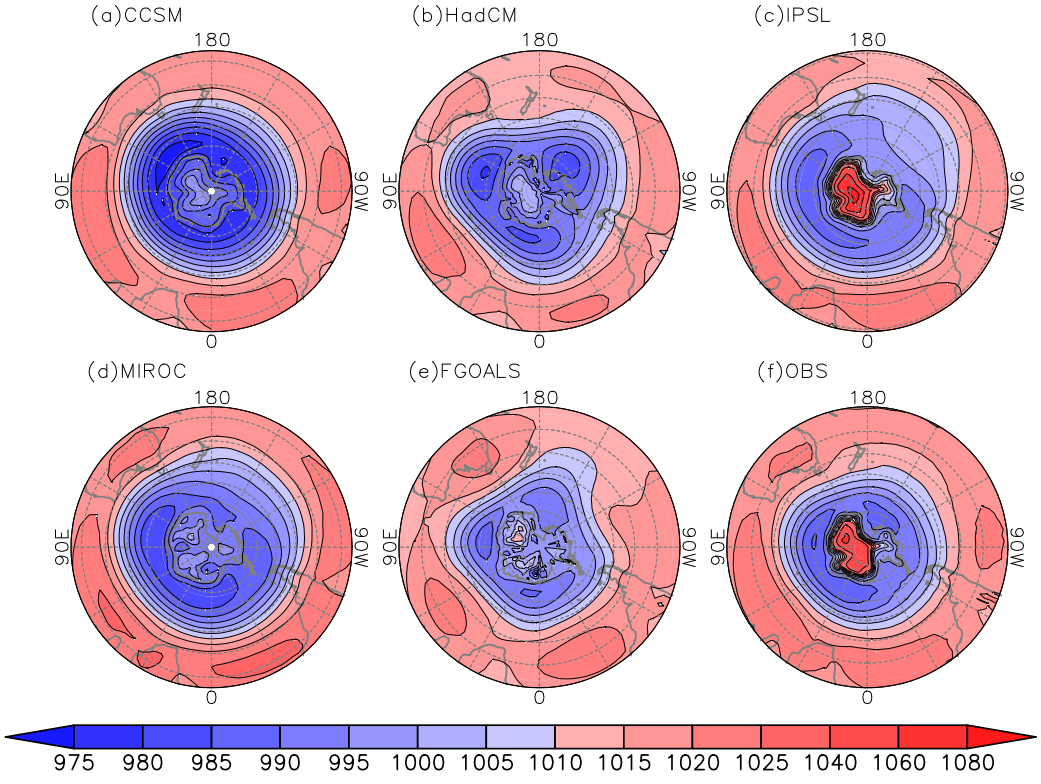

Fig. 1. Climatology of JJA SLP according to the five models for the PI and observations. The contour interval is 500 Pa.

Fig. 2. In terms of the geopotential height, only the results of CCSM, MIROC, and FGOALS are included in the comparison due to data availability. In the observed zonal-mean zonal winds, the subtropical westerly jet at 30°S at about 150–300 hPa in the troposphere and the polar night jet at 60°S in the upper stratosphere are distinct and these features are captured in all the models in terms of position and magnitude to a reasonable degree. Note that all the models reproduce the features found in the observation reasonably well as shown in Fig 2. Nevertheless, detailed comparisons show some discrepancies. For example, most of the models reproduce the polar night jet at 60°S in the upper stratosphere as weaker than in observations. In the case of MIROC, the southern subtropical jet is relatively strong compared to other simulations and the polar-front jet is a little weaker than observed. In an idealized multi-level primitive equation model simulation, Lee and Kim (2003) showed that baroclinic wave growth is most favored along the subtropical jet only when the subtropical jet is sufficiently strong. This strong subtropical jet is also consistent with upper-level meridional temperature gradient (Fig. 2h). Except for MIROC, the simulation results and observations exhibit an extended zonal wind region with the signature of the eddydriven jet as illustrated in Lee and Kim (2003).

Figure 3 displays the changes in surface temperature between the LGM and PI. As would be expected from the glacial boundary conditions, the models simulate an overall colder climate over southern high latitudes in the LGM, even

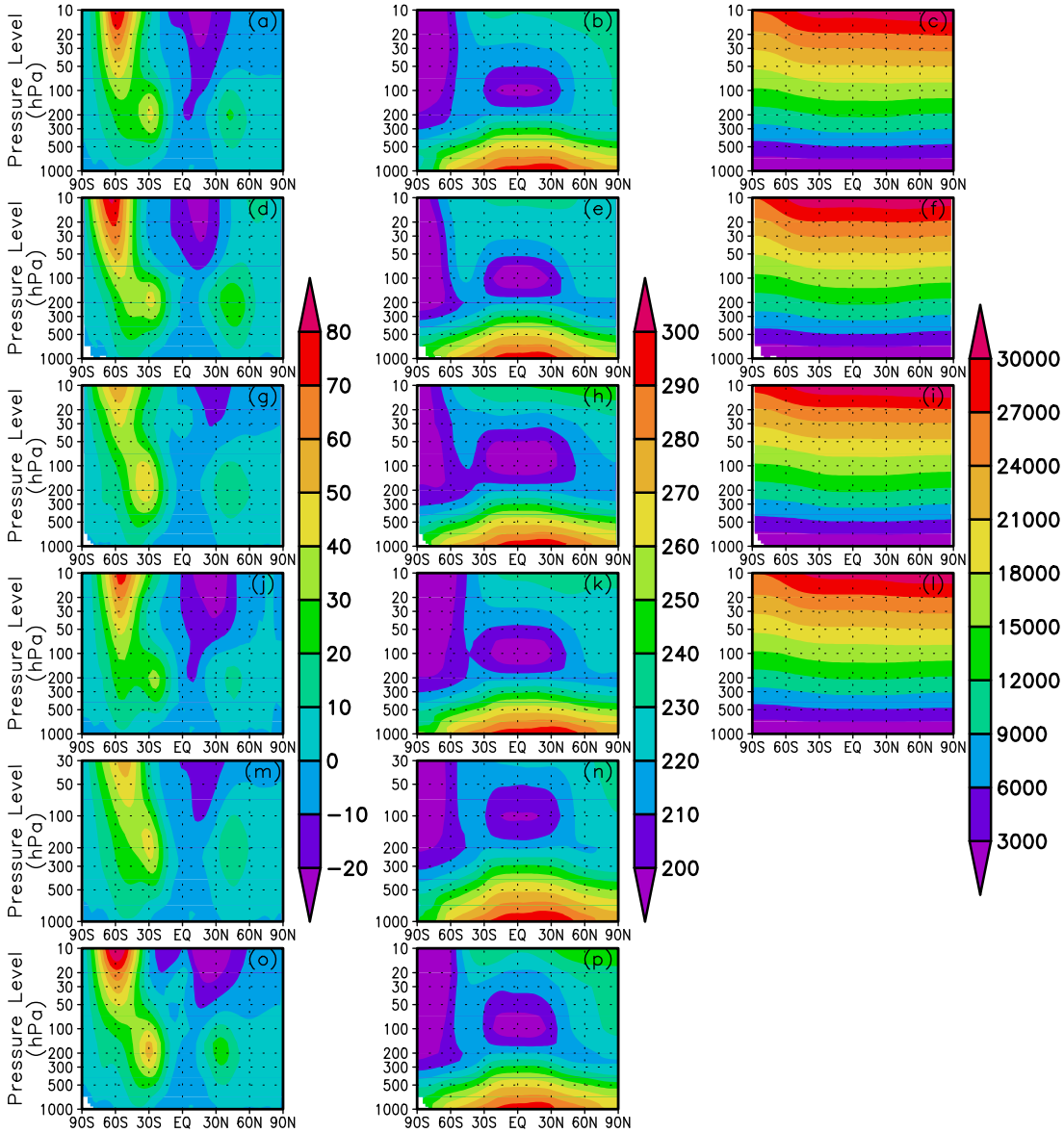

Fig. 2. Austral winter climatology of zonal-mean zonal wind (left), temperature (middle) and geopotential height (right) for (a–c) observations, (d–f) CCSM (g–i) MIROC, (j–l) FGOALS, (m, n) HadCM, and (o, p) IPSL for the PI simulations. Units are m s^{-1} for zonal wind, K for temperature and m for geopotential height.

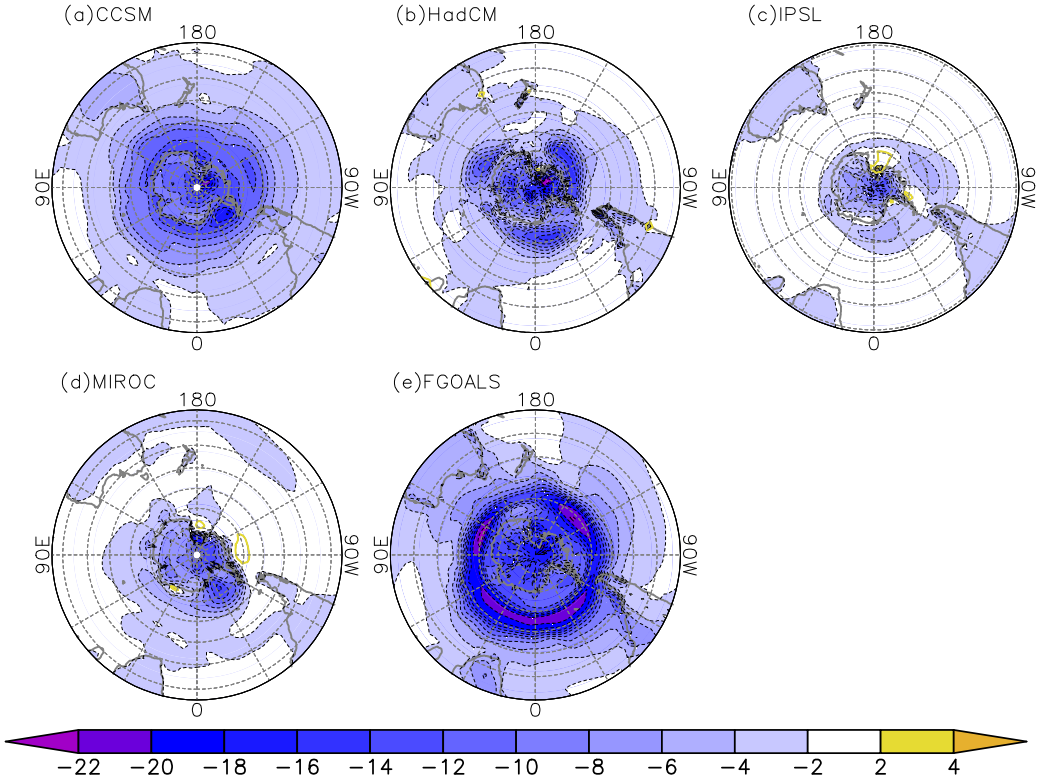

Fig. 3. The modeled changes (LGM minus PI) in JJA surface air temperature. The contour interval is 2 K.

though the degree of surface cooling simulated by the coupled models varies among models, due to the differences in ocean circulation and sea ice changes (Masson-Delmotte et al., 2006) For example, IPSL shows the least surface cooling by less than 8 K over Antarctica, whereas FGOALS shows surface cooling by greater than 20 K. In all the models, the largest surface cooling occurs between the South Pole and West Antarctica, associated with the thickening of the ice sheet by about 2000 m in the LGM. The second largest surface cooling occurs around the Antarctic continent in most of the models, associated with the increase in sea ice extent and associated albedo change. The relatively small surface cooling around Antarctica in IPSL is consistent with the small change in sea ice extent as shown in Fig. 2h in Rojas et al. (2008). Overall, the simulated surface temperature in JJA decreases from about 4.3 K in IPSL to 13 K in FGOALS with a model mean reduction of 8.5 K in high latitudes south of 65°S in the LGM.

There are several proxy reconstructions available for surface temperature change in the LGM over Antarctica. Reconstructed surface cooling in the LGM based on ice core estimates of the Vostock (78°S and 106°E), dome C (75°S and 123°E), and dome Fuji (77°S and 39°E) stations ranges from about −8.5°C to −10.0°C (Petit et al., 1999; Stenni et al., 2001; Kawamura et al., 2007). The degree of multimodel mean surface cooling simulated by the coupled models in these locations is overall within these observed ranges.

The vertical cross section of the differences in zonal-mean zonal wind, temperature, and geopotential height between the LGM and the PI is shown in Fig. 4. In the LGM, the southern part of the SH westerly jet south of 60°S appears to be slightly enhanced, while the northern part of the SH westerly jet north of 60°S becomes substantially weaker from the lower troposphere to the upper stratosphere in all the models except FGOALS. The strengthening (weakening) of the southern (northern) parts of the SH westerly jets in LGM winter is more pronounced in the upper levels above about 300 hPa and toward the higher latitudes.

The change in SH westerly winds in the LGM is associated with the change in temperature. In the LGM, temperature overall decreases in the troposphere, especially in the lower troposphere of high latitudes and upper troposphere of low latitudes. However, in the stratosphere, a relatively large warming is found over southern high and low latitudes and somewhat less warming over midlatitudes. The substantial warming in southern high latitudes at about 60°S leads to the increase in geopotential height relative to lower latitudes, resulting in the increase and decrease in westerly winds in higher and lower latitudes, respectively. Overall, in all models except FGOALS, the SH subtropical jet at about 30°S at 200 hPa and the polar night jet at around 60°S at above the 50 hPa level become substantially weaker.

3.2. *SAM change*

In this study the SAM is defined as the leading EOF of JJA SLP from 20° to 90°S following previous studies (e.g.

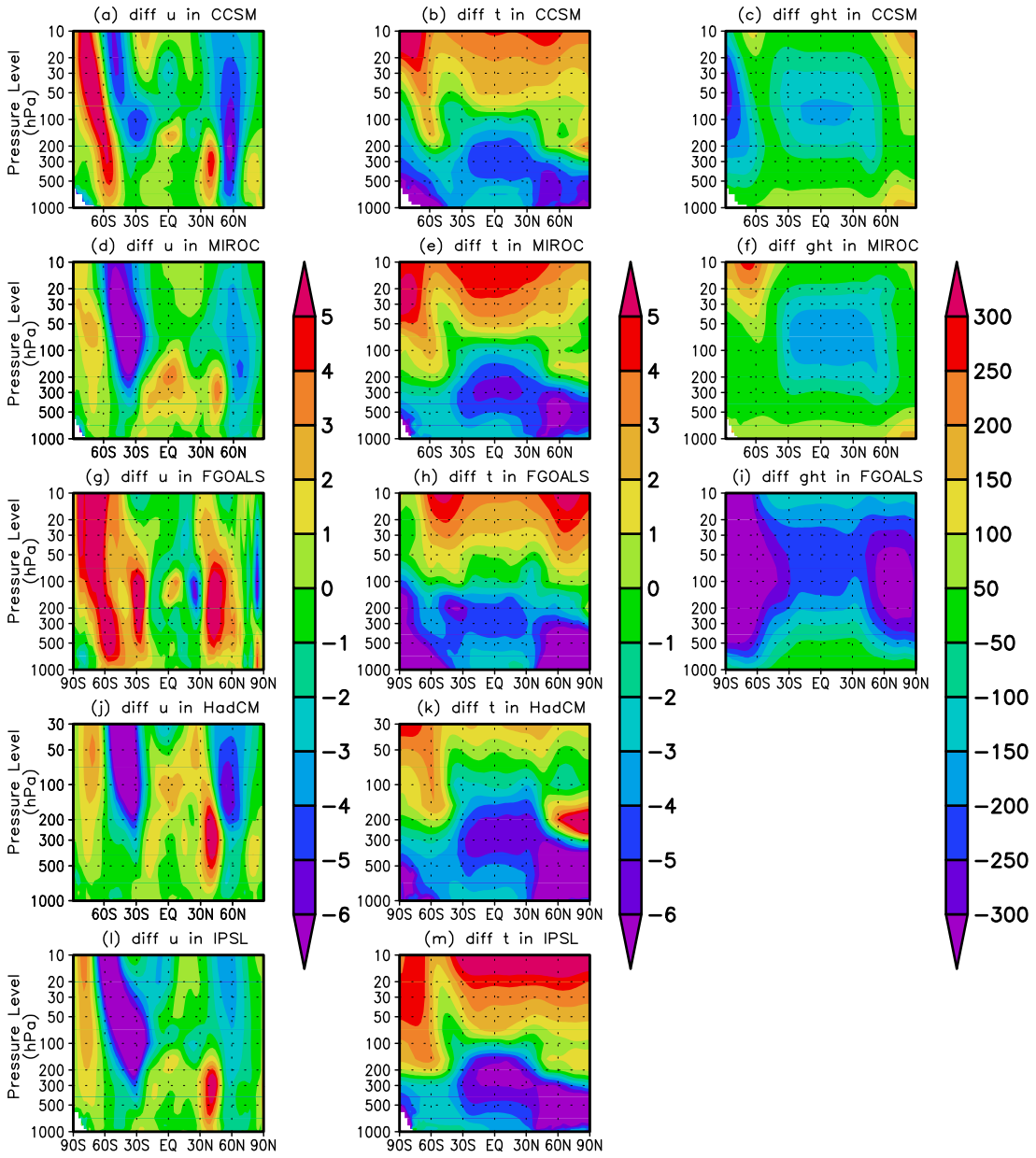

Fig. 4. Differences of austral winter zonal-mean zonal wind (left), temperature (middle) and geopotential height (right) between the LGM and PI for (a–c) CCSM, (d–f) MIROC, (g–i) FGOALS, (j, k) HadCM, and (l, m) IPSL. Units are m s^{-1} for zonal wind, K for temperature and m for geopotential height.

Thompson and Wallace, 2000). The SAM index is defined as the difference in normalized zonal-mean SLP between ∼40°S and 65°S for JJA following Gong and Wang (1999). In the NCEP/NCAR reanalysis data, the leading EOF structure of JJA SLP is characterized by meridional dipoles with negative loadings south of 70°S and positive loadings at midlatitudes of ∼45°S (Fig 5f). The leading EOF structure of JJA SLP is zonally symmetric and characterized by north–south seesaws of atmospheric mass between the high latitudes and the midlatitudes. The leading mode in the NCEP/NCAR reanalysis explains 57% of total variance.

In the PI simulations, all the modeled leading EOFs show annular-like structures and broadly resemble that from the reanalysis (Fig. 5f). Nevertheless, the regional centers of low pressures and circumpolar high pressures vary from model to model. For example, the positive loading is much larger than the observed in the Pacific sector in FGOALS, whereas it is weaker in IPSL. In CCSM, the location of positive loading is similar to that of the reanalysis, although the loading is slightly stronger than that of the reanalysis. In the reanalysis, the deep trough is located between 120°W and 150°W at about 70°S, which is compatible to the Amundsen Sea Low (Turner et al., 2013), but most of the models do not capture the magnitude and positions as in the reanalysis. For exam-

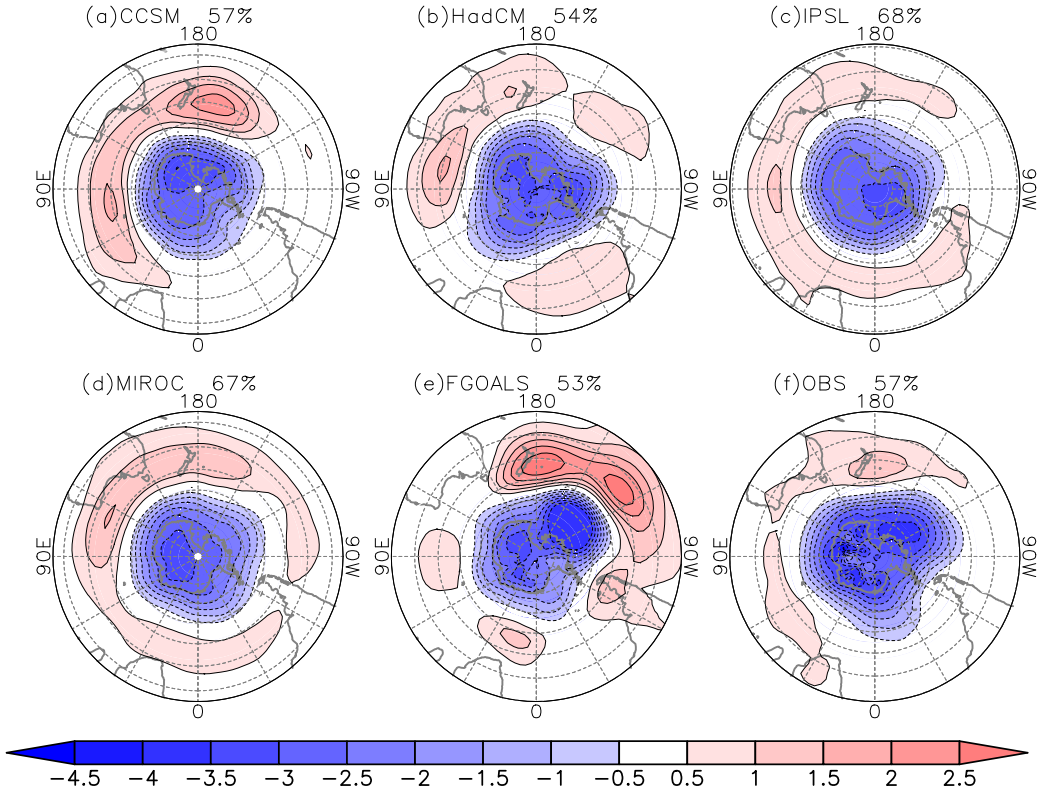

Fig. 5. Leading EOF of JJA SLP during the PI for (a) CCSM, (b) HadCM, (c) IPSL, (d) MIROC, (e) FGOALS, and (f) observations. Percentages of explained variance are shown at the top of each panel. Units are hPa.

ple, in the HadCM experiment, the polar vortex does not extend northward so much as in the reanalysis and in IPSL and MIROC, and the Amundsen Sea Low trough is not captured well. Overall, the modeled leading EOF of JJA SLP explains 53%–68% of total variance in the 5 models (Table 3). The explained variance in observations is within the range of modelsimulated variances.

Figure 6 displays the leading EOF of JJA SLP derived from simulated sea level pressure for the LGM. In the LGM, a difference in the spatial pattern of the leading EOF was found from that of the PI simulations. The positive loading is overall slightly stronger in the LGM than the PI especially in CCSM and HadCM, whereas it is weaker in FGOALS. There is little change in the negative loadings in the LGM simulations compared to those of the PI. The percentages of the explained variance vary from 36% to 74% in the LGM (Table 3). For the FGOALS IPSL, and MIROC cases, the explained SAM variance decreases in the LGM, whereas in CCSM and HadCM the variance is larger in the LGM than those of the PI.

To examine the intensity of the SAM, we calculated standard deviations of the SAM index and refer to them as the amplitude (Table 3). In the LGM, the amplitude of the SAM appears to be overall smaller than in the PI simulation, except for the HadCM case, where the amplitude of the SAM increases slightly in the LGM. Besides the standard deviation (STD) of the SAM indices, we also calculated the mean values of the positive and negative SAM indices and found that these absolute values are overall smaller in the LGM simulations than in the PI cases. Both the standard deviations of SAM indices and mean values of positive and negative SAM indices indicate that in the LGM the SAM was over-

Table 3. SAM statistics for the PI and LGM.

Model	Explained variance		SAM amplitude		Standard deviation of the SAM index	
	0 kyr	21 kyr BP	0 kyr	21 kyr BP	0 kyr	21 kyr BP
CCSM	57%	74%	79	68	2.00	1.82
HadCM3M2	54%	57%	169	146	1.90	1.93
IPSL	68%	59%	177	171	2.07	2.03
MIROC	67%	58%	178	206	2.08	1.59
FGOALS	53%	36%	170	159	2.02	1.66

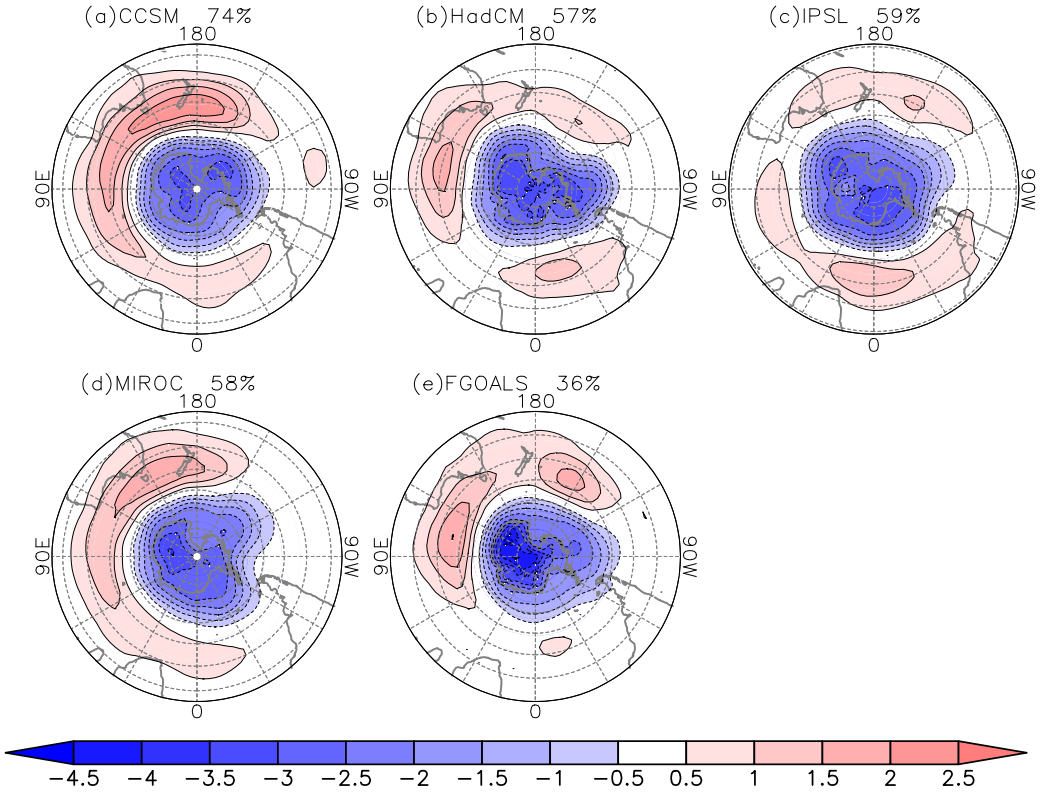

Fig. 6. The same as Fig. 5, but for the LGM. Units are hPa.

all weaker than present, i.e. the amplitude of the SAM was smaller, which in turn implies weaker westerly winds in the SH. The weaker SAM is consistent with the decreased wind intensities from the lower troposphere to upper stratosphere in the LGM during austral winter as shown in Fig. 4. Weaker SH surface westerlies in the LGM were also obtained in previous PMIP2 model data analyses (e.g. Rojas et al., 2008) and are consistent with proxy estimates of the weakening of the Ekman divergence in the SO in the LGM (Sigman and Boyle, 2000; Toggweiler et al., 2006; Anderson et al., 2009; Toggweiler, 2009; Sigman et al., 2010).

In order to measure the effect of the SAM index for the PI on the zonal-mean zonal winds, temperature, and geopotential height, we regressed these variables onto the SAM index (Fig. 7). The model results from CCSM, MIROC and FGOALS only are included in the analysis due to data availability. In the PI simulation, when the SAM index increases by 1 STD the zonal-mean zonal wind increases in mid- to high latitudes from 50° to 60°S and decreases in low latitudes. This feature is common in the three models in terms of its magnitude and location. Analyses indicate that the SAM index is highly correlated with the zonal-mean zonal winds from the surface to the lower stratosphere in both the PI and the LGM. The strong link between the zonal-mean zonal wind and the SAM index is already well known from previous studies (e.g. Thompson and Wallace, 2000) The increase in zonal-mean zonal winds at middle to high latitudes associated with the change in the SAM is due to the reduction in geopotential height in high latitudes and increase in midlatitudes when the SAM index is positive. The reduction in the geopotential height in high southern latitudes is in turn associated with the cooling through the atmospheric column when the SAM is in positive phase

In the LGM, the impact of the SAM on the winds, temperature, and geopotential height is stronger in CCSM and MIROC, but weaker in FGOALS (Fig 8). For example, in CCSM the zonal-mean zonal winds increase substantially by more than 1.5 m s^{-1} per 1 STD of the SAM index above the 500 hPa level up to the top of the stratosphere. The marked increase in zonal-mean zonal winds is again due to the marked reduction in geopotential height in high southern latitudes associated with the remarkable cooling from the midlatitudes toward the high latitudes In MIROC, the zonal-mean zonal winds are slightly stronger in the LGM than in the PI in association with the SAM index, whereas in FGOALS the zonal-mean zonal winds are overall slightly weaker in high-southern latitudes, due to the increase in geopotential height in the LGM.

One dynamical mechanism for maintaining the SAM intensity is the internal interaction between the zonal-mean flow and waves in the atmosphere. To find out what maintained the weaker SAM intensity in the LGM, we examined the activity of stationary Rossby waves. The vertical propagation of the stationary Rossby wave is analyzed using the

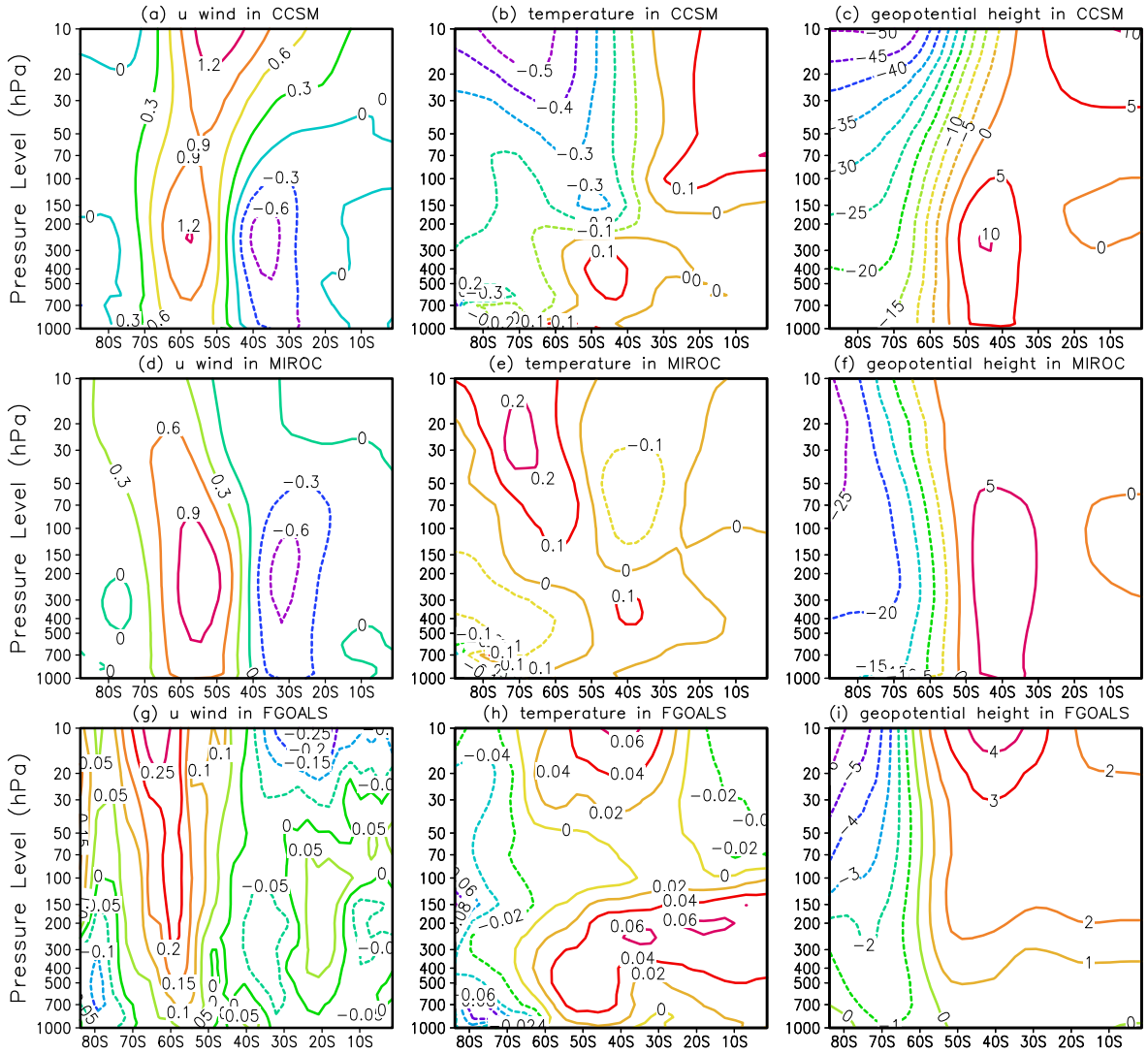

Fig. 7. Zonal-mean zonal wind (a, d, g), temperature (b, e, h) and geopotential height (c, f, i) regressed on the standardized AO index for CCSM (upper panels), MIROC (middle panels) and FGOALS (lower panels) during the PI. Units are m s^{-1}, K, and m per STD of the respective index time series.

Eliassen–Palm (EP) flux defined by Plumb (1985) Following Andrews and McIntyre (1976), the components of the EP flux are written as

$$F_y = -\rho_0 a \cos\varphi \overline{u'v'}\ , \quad F_z = \rho_0 a \cos\varphi f \left(\frac{\overline{v'T'}}{S}\right)\ ,$$

where ρ_0 is air density; a is the radius of the Earth; ϕ is latitude; f is the Coriolis parameter; u and v are zonal and meridional wind components; T is the temperature; and $S = \partial\overline{T}/\partial z + \kappa\overline{T}/H$, where H is the scale height and $\kappa = R_d/c_p$, with R_d being the gas constant and c_p the specific heat of the air. Overbars and primes represent the zonal mean and departures from the zonal mean, respectively.

Figure 9 displays the vertical section of the observed and simulated winter mean EP flux. The observed data to estimate the EP flux are from NCEP/NCAR reanalysis monthly data. In the observation, the flux is upward in the lower and mid troposphere and the flux is especially stronger at around 70°S in the lower troposphere propagating upward into the upper stratosphere. A similar feature is obtained in all the models at lower levels, but the strongest upward flux is located slightly to the north compared to that of the observed, especially in the case of FGOALS. In the upper stratosphere, the EP flux simulated in CCSM is similar to that of the observed, but it is weaker in MIROC and FGOALS.

In the LGM simulation, the upward EP flux at lower levels is weaker than that of the PI case in CCSM and FGOALS, but stronger in MIROC (Fig. 10). In the upper levels, on the other hand, the upward EP flux is strengthened in all models. The stronger upward EP flux in the upper levels decelerates the westerly zonal-mean zonal winds at mid- to high latitudes shown in Fig 4 and seems to maintain the weaker SAM state which is consistent with the overall smaller LGM SAM amplitude in Table 3. The increase in EP flux leads

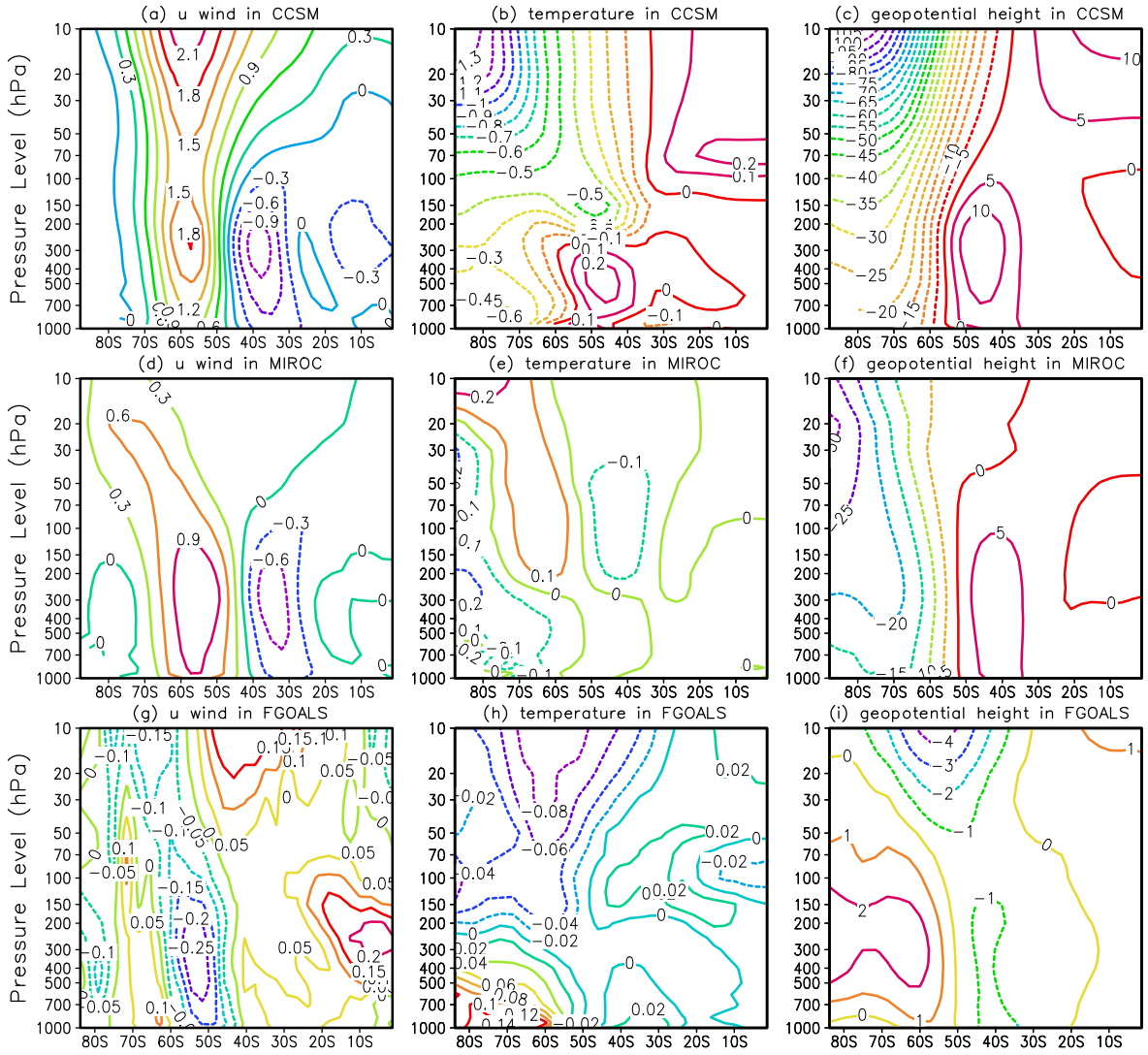

Fig. 8. The same as Fig. 7, but for the LGM.

to the increase in temperature and the geopotential height in the upperlevel high latitudes as shown in Fig 4. This feature is clear in the CCSM and MIROC results, but in the case of FGOALS the upward flux increases in the midlatitudes and this leads to the larger increase in temperature in the midlatitudes than in the high latitudes (Fig. 4h). This results in slightly different zonal-mean zonal wind structure (Fig. 4g) from those in CCSM (Fig. 4a) and MIROC (Fig. 4d).

In the LGM, the EP flux is overall strengthened as shown in Fig. 10. In general, stationary Rossby waves are generated by both topography and thermal contrast (Andrews and McIntyre, 1976). The role of topography and thermal contrast in the EP flux is broadly well known in the NH (Ringler and Cook, 1999), but in the SH the cause of the EP flux modulation remains uncertain. Some studies have suggested that eddy forcing is more important in strengthening the EP flux than topography and thermal contrast (e.g. Karoly et al., 1989), but others suggest the importance of thermal contrast, mainly through a change in sea surface temperature (Hu and Fu, 2009) In the NH, Eurasian snow cover change in the fall is known to amplify the orographicallyinduced upward EP flux in winter by inducing cooling in the lower troposphere (Saito et al., 2001; Cohen et al., 2007; Lü et al., 2008, 2010). In order to check the effect of the snow change in the autumn, which increases in the LGM according to all the models, on the change in EP flux, we estimated the correlation of winter zonal-mean wave activity flux with the autumn increased snow depth in the LGM (Fig. 11). In response to the increase in snow, the wave activity appears to increase at high southern latitudes from the lower troposphere to the stratosphere in the CCSM and MIROC results, but in FGOALS it increases in the troposphere and decreases in the stratosphere. Comparison to Fig 10 indicates that the increase in EP flux in the CCSM and MIROC results is in part related to the increase in snow in the LGM, but in FGOALS the increase in snow does not influence the change in EP flux.

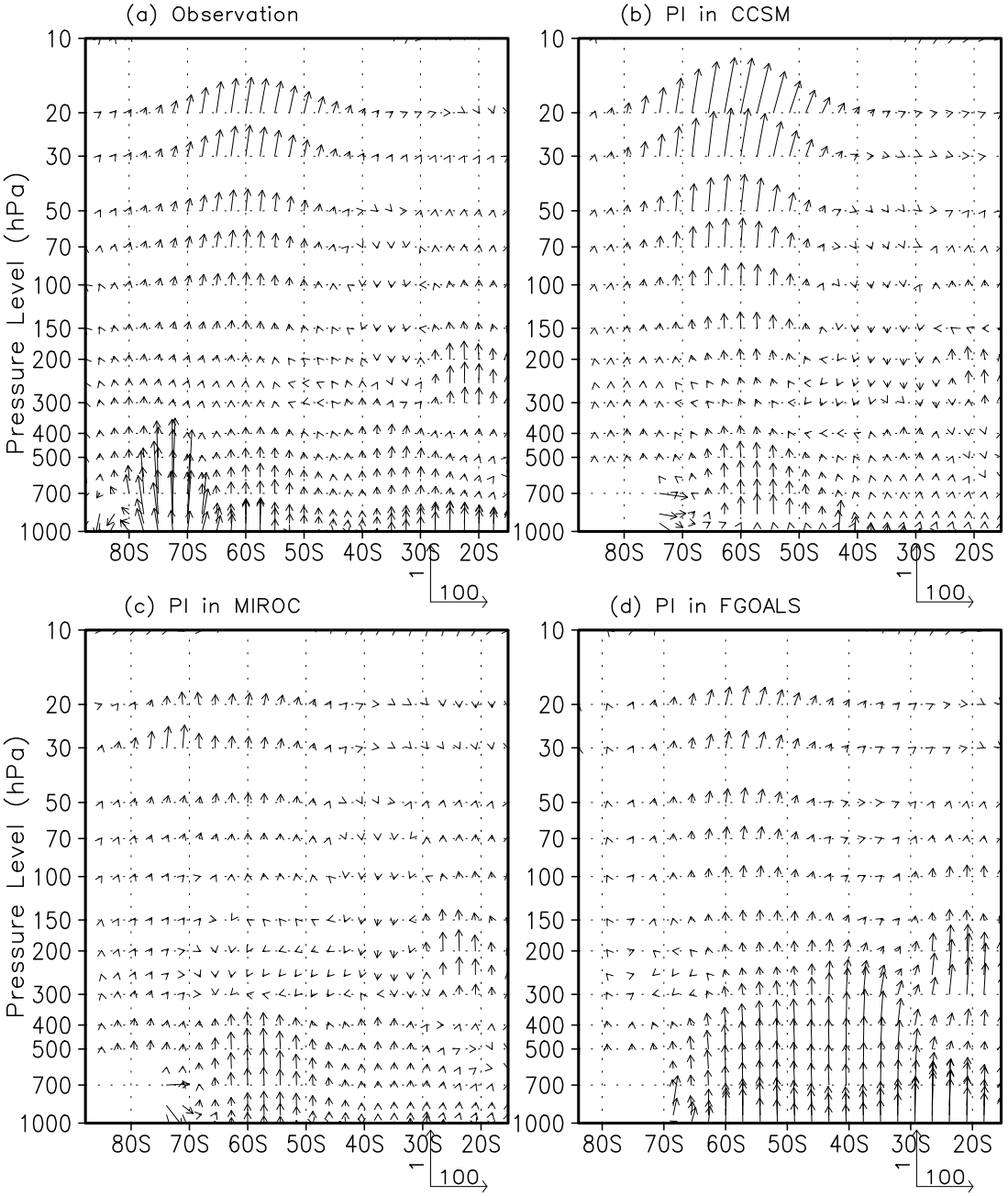

Fig. 9. EP flux cross sections of Rossby waves for the PI: (a) average for 49 winters from the NCEP/NCAR reanalysis, (b) 25 winters from CCSM, (c) 50 winters from MIROC, and (d) 50 winters from FGOALS. Units are $m^2\ s^{-2}$. The horizontal (vertical) scale of arrows is shown at the bottom of the panels and represents 100 (1.0) $m^2\ s^{-2}$.

4. Discussion

The model results indicate that the SAM intensity was weaker in the LGM than present and the weaker SAM intensity was overall consistent with the SH westerly winds in the lower troposphere and stratosphere. However, the strength of the westerly winds over the Southern Ocean during glacial times remains highly uncertain. Some proxy records, such as dust concentrations, including sea-salt chlorides, recorded in Antarctic ice cores (74°S, 124°E; 78°S, 106°E), suggest an enhanced atmospheric circulation with a drier climate than at present in the southern high latitudes (Petit et al., 1981; De Angelis et al., 1987), whereas some authors have claimed that the SO westerly winds were intensified in the LGM due to an increase in the equator-to-pole temperature gradient (e.g. Keeling and Visbeck, 2001). However, low-level winds generally depend on regional temperature gradient rather than global-scale temperature change, as seen in Fig. 3. Some recent proxy estimates have shown that the wind-driven upwelling was enhanced after the termination of the last ice age in the SO (Anderson et al., 2009) and this result indicates weaker westerly winds during the LGM. In LGM climate

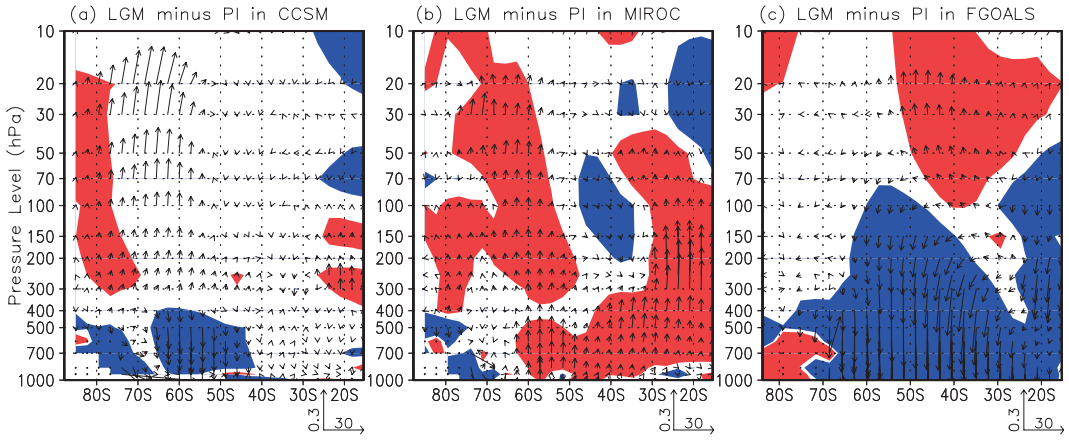

Fig. 10. Changes in the vertical propagation of Rossby waves for the LGM compared to the PI in (a) CCSM, (b) MIROC and (c) FGOALS simulations. Shaded areas indicate significant changes at the 95% level, estimated by a local Student's *t*-test. The horizontal (vertical) scale of arrows is shown at the bottom of the panels and represents 30 (0.3) m^2 s^{-2} The red-colored shading denotes upward-propagating Rossby waves, while the blue-colored shading denotes downward propagation.

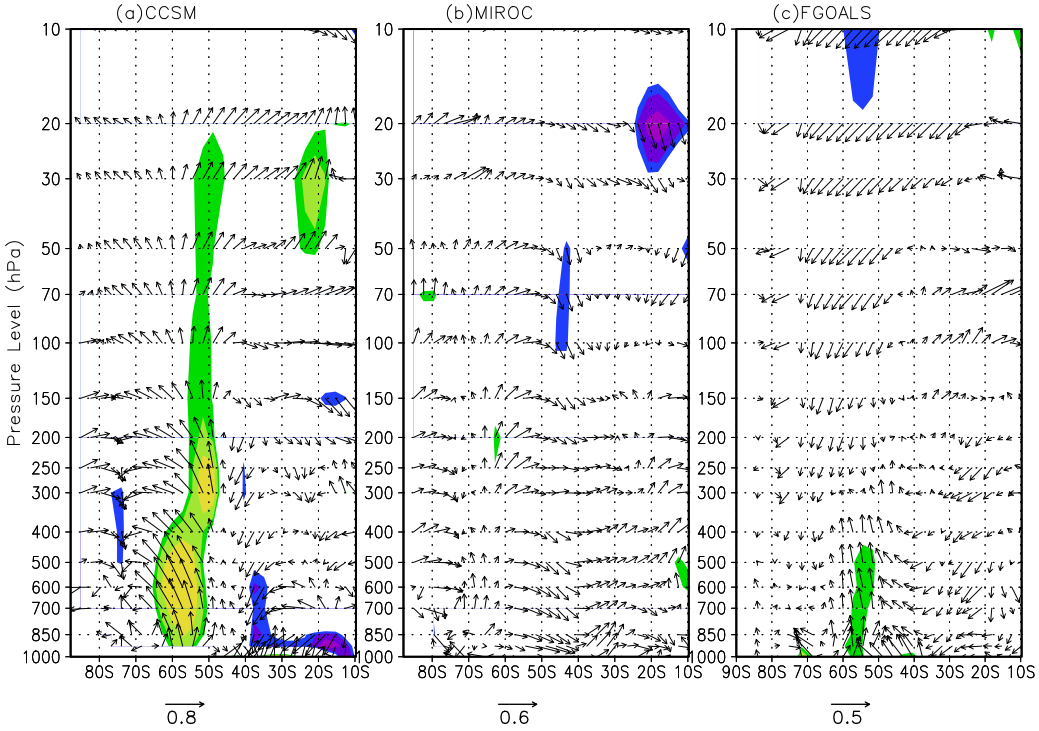

Fig. 11. The regression coefficients of LGM winter zonal-mean WAF (arrows) on the increment of autumn snow depth indices between the LGM and PI for (a) CCSM, (b) MIROC and (c) FGOALS. Shaded areas indicate the 90%, 95%, and 99% confidence levels. The horizontal (vertical) scale of arrows is shown at the bottom. Units are m^2 s^{-2}.

simulations using the NCAR CCM3 AGCM and using the CCCma coupled model, Kim and Lee (2009) and Kim et al. (2003) reported 20%–30% weaker SH westerly winds and an equatorward shift by several degrees An equatorward shift in model results was also obtained by Droset et al. (2007), but more models have shown a poleward shift of SH westerly winds (e.g. Wyrwoll et al., 2000; Kitoh et al., 2001; Sime et al., 2013).

The weaker SH westerly winds in the LGM mirror the intensification of winds under a warm climate background. For example, using the Geophysical Fluid Dynamics Laboratory (GFDL) coupled general circulation model, Kushner et al. (2001) predicted intensified westerly winds from the surface to 250 hPa over the SH in the 21st century. Yin (2005)

and Fyfe and Saenko (2006) analyzed IPCC-reported climate models and obtained a remarkably consistent strengthening and poleward shifting of the zonal wind axis through the 20th and 21st centuries. The latitudinal displacement of the westerly axis in the LGM as a mechanism to illustrate the reduction of atmospheric CO_2 concentration has received much attention in the literature. For example, by analyzing lacustrine palynologic records along the western Andean front of Chile, McCulloch et al. (2000) obtained a northward displacement of westerlies during glacial times. By analyzing pollen types containing information on vegetation migration near the tip of South America, Moreno et al. (1999) also suggested that SO westerly winds shifted northward by 7°–10° in the LGM. Other studies have also suggested a glacial northward displacement of westerly winds in the SO (Heusser, 1989; Sigman and Boyle, 2000; Toggweiler et al., 2006; Anderson et al., 2009; Toggweiler, 2009; Sigman et al., 2010). A northward displacement of SH westerlies by approximately 3°–4° was obtained in some previous model studies of the LGM (e.g. Kim et al., 2003; Kim and Lee, 2009). However, contrasting results exist. For example, Markgraf (1987, 1989) suggested a southward shift of the mean position of glacial SH westerly winds. In the PMIP2 LGM simulations, the axis of the strongest SH westerly winds is located at almost the same position as that of the PI and this has been noted in a previous PMIP2 model analysis (Rojas et al., 2008) Building on the analysis by Rojas et al. (2008), we included the FGOALS model results in our study, and these additional model results confirm the conclusion that the SAM associated with SH westerlies was weaker in the LGM.

The strength of the SH westerly and its position during the LGM is critical with respect to atmospheric CO_2 concentrations associated with the inhibition of CO_2-rich deep ocean water reaching the upper layer and eventually the atmosphere. Regarding the position of the maximum SH westerly winds, model–data and even some model–model discrepancies still exist. More proxy evidence and model studies are necessary to draw a clearer conclusion in terms of the strength and position of the SH westerly winds during the LGM. Our analyses of the LGM simulation results suggest that the SH westerly winds from the lower troposphere to the upper stratosphere were substantially weaker in the LGM, but the axis of the SH westerly winds was almost at the same position as present.

5. Summary and conclusion

In this study we investigated the atmospheric changes in the SH during the LGM using data from PMIP2 coupled model simulations. Results from five coupled models (CCSM, HadCM, MIROC3.2, IPSL-CM4, and FGOALS) were used. In the LGM experiment, ICE-5G ice sheet topography and associated sea level lowering were implemented. The atmospheric CO_2 concentration was reduced to 185 ppm in the LGM simulation from 280 ppm in the PI simulation. It was found that all models reproduce the observed features to a reasonable degree in the PI simulations. With the implementation of the LGM conditions, surface temperature decreases by more than 8°C over the Antarctic continent and this is within the range of surface cooling from proxy evidence. Note that we used PMIP2 model outputs instead of PMIP3 results, which constitute the state-of-the-art, latest version. It is therefore necessary in the future to use PMIP3 results to investigate LGM SAM changes and the underlying mechanisms.

In the LGM simulations, it was found that the majority of models exhibit a weaker SAM intensity than in the PI simulation and the weaker SAM intensity is consistent with the weaker zonal-mean zonal winds, especially in the middle and upper levels. The weaker SAM intensity is associated with the increase in geopotential height in high latitudes due to the increase in temperature in the upper atmosphere. Analysis of the changes in EP flux indicated that the upward planetary Rossby wave activity was enhanced from the middle to the upper atmosphere in the LGM and the enhanced upward EP flux would have led to the increase in the upperlevel temperature in high southern latitudes.

In conclusion, the SAM appears to have been weaker than present during the LGM and the weakening of the SAM was consistent with a reduction of SH westerly winds. Weaker SH westerly winds in the LGM are supported by some lines of proxy evidence as well as the increase in SH wind intensity under global warming.

Acknowledgements. We would like to thank the PMIP2 members for providing the data. Hyesun CHOI at the Korea Polar Research Institute (KOPRI) is acknowledged for her help in proofreading the manuscript. This study was supported by the "Investigation of Climate Change Mechanism by Observation and Simulation of Polar Climate Change for the Past and Present" project (PE14010) of the KOPRI, the Special Project of Basic Science and Technology (2011FY120300), and the Korea Meteorological Administration Research and Development Program under Grant CATER 2012-3061 (PN13010). This work was also supported by the Jiangsu Collaborative Innovation Center for Climate Change.

REFERENCES

Anderson, R. F., S. Ali, L. I. Bradtmiller, S. H. Nielsen, M. Q. Fleisher, B. E. Anderson, and L. H. Burckle, 2009: Wind-driven upwelling in the southern ocean and the Deglacial Rise in Atmospheric CO_2. *Science*, **323**, 1443–1448.

Andrews, D. G., and M. E. McIntyre, 1976: Planetary waves in horizontal and vertical shear: The general Eliassen-Palm relation and the mean zonal acceleration. *J. Atmos. Sci.*, **33**, 2031–2048.

Berger, A. L., 1978: Long-term variations of caloric insolation resulting from the Earth's orbital elements. *Quaternary Research* **9**, 139–167.

Braconnot, P., and Coauthors, 2007a: Results of PMIP2 coupled simulations of the Mid-Holocene and Last Glacial Maximum—Part 1: Experiments and large-scale features. *Climate of the Past*, **3**, 261–277.

Braconnot, P., and Coauthors, 2007b: Results of PMIP2 coupled simulations of the Mid-Holocene and Last Glacial

Maximum—Part 2: Feedbacks with emphasis on the location of the ITCZ and mid- and high latitudes heat budget. *Climate of the Past*, **3**, 261–277.

Cai, W., and T. Cowan, 2007: Trends in southern hemisphere circulation in IPCC AR4 Models over 1950-99: Ozone Depletion versus Greenhouse Forcing. *J. Climate*, **20**, 681–693, doi: 10.1175/JCLI4028.1.

Chapman, W. L., and J. E. Walsh, 2007: A Synthesis of Antarctic Temperatures. *J. Climate*, **20**, 4096–4117.

Cohen, J., M. Barlow, P. Kushner, and K. Saito, 2007: Stratosphere-troposphere coupling and links with Eurasian land surface variability. *J. Climate*, **20**, 5335–5343.

Crucifix, M., P. Braconnot, S. P. Harrison, and B. Otto-Bliesner, 2005: Second phase of paleoclimate modelling intercomparison project. *Eos Trans. Amer. Geophys. Union*, **86**, 264.

Dällenbach, A., T. Blunier, J. Flückiger, B. Stauffer, J. Chappellaz, and D. Raynaud, 2000: Changes in the atmospheric CH_4 gradient between Greenland and Antarctica during the Last Glacial and the transition to the Holocene. *Geophys. Res. Lett.*, **27**, 1005–1008.

De Angelis, M., N. I. Barkov, and V. N. Petrov, 1987: Aerosol concentrations over the last climatic cycle (160 kyr) from an Antarctic ice core. *Nature*, **325**, 318–321.

Droset, F., J. Renwick, B. Bhaskarane, H. Oliver, and J. McGregor, 2007: Features of the zonal mean circulation in the southern hemisphere during the Last Glacial Maximum. *J. Geophys. Res*., **112** D2, doi: 10.1029/2005JD006811.

Flückiger, J., A. Dällenbach, T. Blunier, B. Stauffer, T. F. Stocker, D. R. Raynaud, and J.-M. Barnola, 1999: Variations in atmospheric N_2O concentration during abrupt climatic changes. *Science*, **285**, 227–230.

Fyfe, J. C., G. J. Boer, and G. M. Flato, 1999: The arctic and antarctic oscillations and their projected changes under global warming. *Geophys. Res. Lett*., **26**, 1601–1604.

Fyfe, J. C., and O. A. Saenko, 2006: Simulated changes in the extratropical Southern Hemisphere winds and currents. *Geophys. Res. Lett*., **33**, L06701, doi: 10.1029/2005GL025332.

Gillett, N. P., and D. W. J. Thompson, 2003: Simulation of recent Southern Hemisphere climate change. *Science*, **302**, 273–275.

Gillett, N. P., T. D. Kell, and P. D. Jones, 2006: Regional climate impacts of the Southern annular Mode. *Geophys. Res. Lett*., **33**(23), L23704, doi: 10.1029/2006GL027721.

Gong, D Y. and S. Wang, 1999: Definition of Antarctic oscillation index. *Geophys. Res. Lett*, **26**, 459–462.

Gordon, C., C. Cooper, C. A Senior, H. Banks, J. M. Gregory, T. C. Johns, J. F. B. Mitchell, and R. A. Wood, 2000: The simulation of SST, sea ice extents and ocean heat transports in a version of the Hadley Centre coupled model without flux adjustments. *Climate Dyn*., **16**, 147–168.

Hall, A., and M. Visbeck, 2002: Synchronous variability in the Southern Hemisphere atmosphere, sea ice, and ocean resulting from the Annular Mode. *J. Climate*, **15**, 3043–3057.

Harrison, S. P., P. Braconnot, S. Joussaume, C. D. Hewitt, and R. J. Stouffer, 2002: Fourth international workshop of the Palaeoclimate Modelling Intercomparison Project [PMIP]: launching PMIP Phase II. *Eos Trans. Amer. Geophys. Union*, **83**, 447.

Heusser, C. J., 1989: Southern westerlies during the Last Glacial Maximum. *Quaternary Research*, **31**, 423–425.

Hu, Y., and Q. Fu, 2009: Stratospheric warming in Southern Hemisphere high latitudes since 1979. *Atmospheric Chemistry and Physics*, **9**, 4329–4340.

Hurrell, J. W., and H. van Loon, 1994: A modulation of the atmospheric annual cycle in the Southern Hemisphere. *Tellus*, **46**, 325–338.

Jiang, D. B., and X. M. Lang, 2010: Last glacial maximum East Asian monsoon: Results of PMIP simulations. *J. Climate*, **23**, 5030–5038.

Jiang, D. B., X. M. Lang, Z. P. Tian, and D. L. Guo, 2011: Last glacial maximum climate over China from PMIP simulations. *Palaeogeography, Palaeoclimatology, Palaeoecology*, **309**, 347–357.

Jones, J. M., and M. Widmann, 2003: Instrument- and tree-ring-based estimates of the Antarctic Oscillation. *J. Climate*, **16**, 3511–3524.

Joussaume, S., and K. E. Taylor, 2000: Paleoclimate modeling intercomparison project (PMIP). *Proceedings of the third PMIP workshop WCRP-111*, edited by P. Braconnot, Canada, 9-24.

K-1 Model Developers, 2004: K-1 coupled model (MIROC) description. K-1 Technical Report No. 1 H. Hasumi and S. Emori, Eds, Center for Climate System Research, University of Tokyo, 34 pp.

Kageyama, M., and Coauthors, 2006: Last Glacial Maximum temperatures over the North Atlantic, Europe and western Siberia: a comparison between PMIP models, MARGO sea-surface temperatures and pollen-based reconstructions. *Quaternary Science Reviews*, **25**, 2082–2102.

Karoly, D. J., 2003: Atmospheric science: Ozone and climate change. *Science*, **302**, 236–237, doi: 10.1126/science.1090851.

Karoly, D. J., R. A. Plumb, and M. F. Ting, 1989: Examples of the horizontal propagation of quasi-stationary waves. *J. Atmos. Sci*., **46**, 2902–2811.

Karpechko, A. Y., N. P. Gillett, L. J. Gray, and M. Dall'Amico, 2010: Influence of ozone recovery and greenhouse gas increases on Southern Hemisphere circulation. *J. Geophys. Res.* **115**, D22117, doi: 10.1029/2010JD014423.

Kawamura, K., and Coauthors, 2007: Northern hemisphere forcing of climatic cycles in Antarctica over the past 360, 000 years. *Nature*, **448**, 912–916.

Keeling, R. F., and M. Visbeck, 2001: Antarctic stratification and glacial CO_2. *Nature*, **412**, 605–606.

Keeley, S. P. E., N. P. Gillett, D. W. J. Thompson, S. Solomon, and P. M. Forster, 2007: Is Antarctic climate most sensitive to ozone depletion in the middle or lower stratosphere? *Geophys. Res. Lett*., **34**, L22812, doi: 10.1029/2007GL031238.

Kim, S.-J., and B. Y. Lee, 2009: Westerly winds in the Southern Ocean during the Last glacial maximum simulated in CCM3. *Ocean and Polar Res*., **31**(4), 297–304.

Kim, S-J., G. M., Flato, and G. J. Boer, 2003: A coupled climate model simulation of the Last Glacial Maximum, Part 2: Approach to equilibrium. *Climate Dyn.*, **20**, 635–661.

Kitoh, A., S. Murakami, and H. Koide, 2001: A simulation of the Last Glacial Maximum with a coupled atmosphere-ocean GCM. *Geophys. Res. Lett.*, **28**, 2221–2224.

Kushner, P. J., I. M. Held, and T. L. Delworth, 2001: Southern Hemisphere atmospheric circulation response to global warming. *J. Climate*, **14**, 2238–2249.

Kwok, R., and J. C. Comiso, 2002: Spatial patterns of variability in Antarctic surface temperature: Connections to the Southern Hemisphere Annular Mode and the Southern Oscillation. *Geophys. Res. Lett*., **29**, doi: 10.1029/2002GL015415.

Laîné, A., and Coauthors, 2008: Northern hemisphere storm-tracks during the Last Glacial Maximum in the PMIP2

Ocean-Atmosphere coupled models: energetic study, seasonal cycle, precipitation. *Climate Dyn.*, **32**, 593–614, doi: 10.1007/s00382-008-0391-9.

Lee, S., and H.-K. Kim, 2003: The dynamical relationship between subtropical and eddy-driven jets. *J. Atmos. Sci.*, **60**, 1490–1503.

Lefebvre, W., H. Goosse, R. Timmermann, and T. Fichefet, 2004: Influence of the Southern Annular Mode on the sea-ice-ocean system. *J. Geophys. Res.*, **109**, C090005, doi: 10.1029/2004JC002403.

Li, C., and D. S. Battisti, 2008: Reduced Atlantic storminess during last glacial Maximum: Evidence from a coupled climate model. *J. Climate*, **21**(14), 3561–3579, doi: 10.1175/2007JCLI2166.1.

Lü, J.-M., J. H. Ju, S.-J. Kim, J. Z. Ren, and Y. X. Zhu, 2008: Arctic Oscillation and the autumn/winter snow depth over the Tibetan Plateau. *J. Geophys. Res.*, **113**, D14117, doi: 10.1029/2007JD009567.

Lü, J.-M., S.-J. Kim, A. Abe-Ouchi, Y. Yu, and R. Ohgaito, 2010: Arctic Oscillation during the mid-Holocene and last glacial maximum from PMIP2 coupled model simulations. *J. Climate*, **23**(14), doi: 10.1175/2010JCLI3331.1.

Markgraf, V., 1987: Paleoenvironmental changes at the northern limit of the subantarctic Nothofagus forest, Lat 37°S, Argentina. *Quaternary Research*, **28**, 119–129.

Markgraf, V., 1989: Southern westerlies during the Last Glacial Maximum-reply. *Quaternary Research*, **31**, 426–432.

Marshall, G. J., 2003: Trends in the Southern annular mode from observations and reanalyses. *J. Climate*, **16**, 4134–4143.

Marshall, G. J., and W. M. Connolley, 2006: Effect of changing Southern Hemisphere winter sea surface temperatures on Southern Annular Mode strength. *Geophys. Res. Lett.*, **33**(17), L17717, doi: 10.1029/2006GL026627.

Marshall, G. J., P. A. Stott, J. Turner, W. M. Connolley, J. C. King, and T. A. Lachlan-Cope, 2004: Causes of exceptional atmospheric circulation changes in the Southern Hemisphere. *Geophys. Res. Lett.*, **31**, L14205, doi: 10.1029/2004GL019952.

Marti, O., and Coauthors, 2005: The New IPSL Climate System Model: IPSL-CM4. Rep. 26, Institute Pierre Simon Laplace des Sciences de l' Environment Global, Paris, p84.

Masson-Delmotte, V., and Coauthors, 2006: Past temperature reconstructions from deep ice cores: relevance for future climate change. *Climate of the Past*, **2**, 145–165.

McCulloch, R. D., M. J. Bently, R. S. Purves, N. R. J. Hulton, D. E. Sugden, and C. M. Clapperton, 2000: Climate inferences from glacial and palaeoecological evidence at the last glacial termination, southern South America. *Journal of Quaternary Science*, **15**, 409–417.

Meredith, M. P., P. L. Woodworth, C. W. Hughes, and V. Stepanov, 2004: Changes in the ocean transport through Drake Passage during the 1980s and 1990s, forced by changes in Southern Annular Mode. *Geophys. Res. Lett*, **31**, doi: 10.1029/2004GL021169.

Monaghan, A. J., D. H. Bromwich, W. Chapman, and J. C. Comiso, 2008: Recent variability and trends of Antarctic near-surface temperature. *J. Geophys. Res.*, **113**, D04105, doi: 10.1029/2007JD009094.

Monnin, E., A. Indermühle, A. Dällenbach, J. Flückiger, B. Stauffer, T. F. Stocker, D. Raynaud, and J. M. Barnola, 2001: Atmospheric CO_2 concentration over the last glacial termination. *Science*, **291**, 112–114.

Moreno, P. I., T. V. Lowell, G. L. Jacobson Jr., and G. H. Denton, 1999: Vegetation and climate changes during the last glacial maximum and last termination in the Chilean Lake District: A case study from Canal de la Puntilla (41°S). *Geografiska Annaler Series A*, **81**, 285–311.

Murakami, S., R. Ohgaito, A. Abe-Ouchi, M. Crucifix, and B. L. Otto-Bliesner, 2008: Global-scale energy and freshwater balance in glacial climate: A comparison of three PMIP2 LGM simulations. *J. Climate*, **21**(19), 5008–5033.

O'Donnell, R., N. Lewis, S. Mcintyre, and I. Condon, 2011: Improved methods for PCA-based reconstructions: Case study using Steig et al. (2009) Antarctic temperature reconstruction. *J. Climate*, **24**, 2099–2115.

Otto-Bliesner, B. L., E. Brady, G. Clauzet, R. Tomas, S. Levis, and Z. Kothavala, 2006a: Last glacial maximum and holocene climate in CCSM. *J. Climate*, **19**, 2526–2544.

Otto-Bliesner, B. L., R. Tomas, E. C. Brady, C. Ammann, Z. Kothavala, and G. Clauzet, 2006b: Climate sensitivity of moderate- and low-resolution versions of CCSM to preindustrial forcings. *J. Climate*, **19**(11), 2567–2583.

Otto-Bliesner, B. L., C. D. Hewitt, T. M. Marchitto, E. Brady, A. Abe-Ouchi, M. Crucifix, S. Murakami, and S. L. Weber, 2007: Last Glacial Maximum ocean thermohaline circulation: PMIP2 model inter-comparison and data constraints. *Geophys. Res. Lett.*, **34**, L12706. doi: 10.1029/2007GL029475.

Otto-Bliesner, B. L., and Coauthors, 2009: A comparison of PMIP2 model simulations and the MARGO proxy reconstruction for tropical sea surface temperatures at last glacial maximum. *Climate Dyn.*, **32**(6), 799–815, doi: 10.1007/s00382-008-0509-0.

Pausata, F. S. R., C. Li, J. J. Wettstein, K. H. Nisancioglu, and D. S. Battisti, 2009: Changes in atmospheric variability in a glacial climate and the impacts on proxy data: a model intercomparison. *Climate of the Past*, **5**, 489–502.

Petit, J. R., M. Briat, and A. Royer, 1981: Ice age aerosol content from East Antarctic ice core samples and past wind strength. *Nature*, **293**, 391–394.

Petit, J. R., and Coauthors, 1999: Climate and atmospheric history of the past 420, 000 years from the Vostok ice core, Antarctica. *Nature*, **399**, 429–436.

Plumb, R. A., 1985: On the three-dimensional propagation of stationary waves. *J. Atmos. Sci.*, **42**(3), 217–229.

Polvani, L. M., M. Previdi, and C. Deser, 2011: Large cancellation, due to ozone recovery, of future Southern Hemisphere atmospheric circulation trends. *Geophys. Res. Lett.* **38**, L04707, doi: 10.1029/2011GL046712.

Ramstein, G., M. Kageyama, J. Guiot, H. Wu, C. Hély, G. Krinner, and S. Brewer, 2007: How cold was Europe at the Last Glacial Maximum? A synthesis of the progress achieved since the first PMIP model-data comparison. *Climate of the Past*, **3**, 331–339.

Ringler, T. D., and K. H. Cook, 1999: Understanding the seasonality of orographically forced stationary waves: Interaction between mechanical and thermal forcing. *J. Atmos. Sci.*, **56**, 1154-1174.

Rojas, M., and Coauthors, 2008: The Southern westerlies during the last glacial maximum in PMIP2 simulations. *Climate Dyn.*, **32**(4), doi: 10.1007/s00382-008-0421-7.

Saito, K., J. Cohen, and D. Entekhabi, 2001: Evolution of atmospheric response to early-season Eurasian snow cover anomalies. *Mon. Wea. Rev.*, **129**, 2746–2760.

Schneider, D. P., C. Deser, and Y. Okumura, 2012: An assessment and interpretation of the observed warming of West Antarc-

tica in the austral spring. *Climate Dyn.*, **38**(1), 323–347, doi: 10.1007/s00382-010-0985-x.

Shindell, D. T., and G. A. Schmidt, 2004: Southern Hemisphere climate response to ozone changes and greenhouse gas increases. *Geophys. Res. Lett.*, **31**, L18209, doi: 10.1029/2004 GL020724.

Sigman, D. M., and E. A. Boyle, 2000: Glacial/interglacial variations in atmospheric carbon dioxide. *Nature*, **407**, 859–869.

Sigman, D. M., M. P. Haon, and G. H. Haug, 2010: The polar ocean and glacial cycles in atmospheric CO_2 concentration. *Nature*, **466**, 47–55.

Silvestri, G. E., and C. S. Vera, 2003: Antarctic Oscillation signal on precipitation anomalies over southeastern South America. *Geophys. Res. Lett.*, **30**(21), 2115–2118, doi: 10.1029/ 2003GL018277.

Sime, L. C., and Coauthors, 2013: Glacial-interglacial changes in Southern Hemisphere westerly winds: Model-data comparison *Quaternary Science Review*, **64** 104–120, doi: 10.1016/ j.quascirev.2012.12.008.

Son, S.-W., and Coauthors, 2008: The impact of stratospheric ozone recovery on the southern hemisphere westerly jet. *Science*, **320**, 1486–1489.

Son, S.-W., and Coauthors, 2010: Impact of stratospheric ozone on Southern Hemisphere circulation change: A multi-model assessment. *J. Geophys. Res.* **115**, D00M07, doi: 10.1029/ 2010JD014271.

Steig, E. J., D. P. Schneider, S. D. Rutherford, M. E. Mann, J. C. Comiso, and D. T. Shindell, 2009: Warming of the Antarctic ice-sheet surface since the 1957 International Geophysical Year. *Nature*, **457**, 459–463, doi: 10.1038/nature07669.

Stenni, B., V. Masson-Delmotte, S. Johnsen, J. Jouzel, A. Longinelli, E. Monnin, R. Röthlisberger, and E. Selmo, 2001: An oceanic cold reversal during the last deglaciation. *Science*, **293**, 2074–2077.

Thompson, D. W. J., and J. M. Wallace, 2000: Annular modes in the extratropical circulation, part I: Month-to-month variability. *J. Climate*, **13**, 1000–1016.

Thompson, D. W. J., and S. Solomon, 2002: Interpretation of recent Southern Hemisphere climate change. *Science*, **296**, 895–899.

Toggweiler, J. R., 2009: Shifting westerlies. *Science*, **323**, 1434–1435.

Toggweiler, J. R., J. L. Russell, and S. R. Carson, 2006: Midlatitude westerlies, atmospheric CO_2, and climate change during the ice ages. *Paleoceanography*, **21**, PA2005, doi: 10.1029/ 2005PA001154.

Turner, J., and Coauthors, 2005: Antarctic climate change during the last 50 years. *Int. J. Climate*, **25**, 279–294.

Turner, J., T. Phillips, J. S. Hosking, G. J. Marshall, and A. Orr, 2013: The Amundsen Sea low. *Int. J. Climatology*, **33**, 1818–1829.

Weber, S. L., and Coauthors, 2007: The modern and glacial overturning circulation in the Atlantic Ocean in PMIP coupled model simulations. *Climate of the Past*, **3**, 51–64.

Wyroll, K.-H., B. Dong, and P. Valdes, 2000: On the position of Southern Hemisphere westerlies at the Last Glacial Maximum: an outline of AGCM simulation results and evaluation of their implications. *Quaternary Science Reviews*, **19**, 881–898.

Yanase, W., and A. Abe-Ouchi, 2007: The LGM surface climate and atmospheric circulation over East Asia and the North Pacific in PMIP2 coupled model simulations. *Climate of the Past*, **3**, 439–451.

Yu, Y. Q., X. H. Zhang, Y. F. Guo, 2004: Global coupled ocean-atmosphere general circulation models in LASG/IAP. *Adv. Atmos. Sci.*, **21**(3), 444–455, doi: 10.1007/ BF02915571.